ACS OMEGA

Article

Cite This: ACS Omega 2019, 4, 18279−18288

http://pubs.acs.org/journal/acsodf

Semiconductor-Microbial Mechanism of Selective Dissolution of Chalcocite in Bioleaching

Biao Wu, Xinlong Yang,* Jiankang Wen, and Dianzuo Wang

National Engineering Laboratory of Biohydrometallurgy, GRINM Group Corporation Limited, Beijing 100088, China

ABSTRACT: Chalcocite-dominant secondary copper ore with a high pyrite content had a rapidly increased iron concentration in the middle and later periods of bioleaching, which increased the difficulty of separating copper and iron ions in the leaching solution. In the two aspects of microbial community succession and energy band theory, the selective dissolution mechanism of chalcocite in this type of copper ore was analyzed and illustrated using experiments and first-principles calculations. The results showed that controlling the solution potential at a lower level was beneficial to the selective leaching of chalcocite, while bacteria promoted the leaching of pyrite and chalcocite simultaneously by oxidizing Fe^{2+} to Fe^{3+} in the solution. Below 700 mV of solution potential, the bacterial community, mainly consisting of *Acidithiobacillus* and *Sulfobacillus*, had a stronger promotion on the selective dissolution of chalcocite. The solution energy level of bioleaching was higher than ideal pyrite but lower than ideal chalcocite, which resulted in the accumulation of electrons on the surface of pyrite and the formation of holes at the top of the chalcocite valence band. When bacteria assisted the oxidation of Fe^{2+} to Fe^{3+} and caused the raise of the solution potential, the difference between the solution energy level and the top of the pyrite valence band would be smaller than the width of the pyrite energy gap. Below 700 mV, the assistance of *Acidithiobacillus* and *Sulfobacillus* on the oxidation of Fe^{2+} was weak. Chalcocite would be selectively dissolved by oxygen and a small amount of Fe^{3+} in the solution. Because of the existence of Fe, Cu, and S vacancies in real minerals, the atomic activity in the Cu−S bond and the Fe−S bond enhanced, and the reaction difficulty between chalcocite, pyrite, and electron acceptors in the solution reduced. The solution potential should be controlled at 600 mV or less to ensure the selective dissolution of chalcocite.

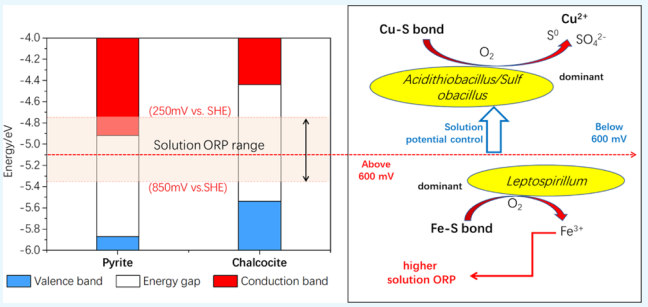

1. INTRODUCTION

Chalcocite (Cu_2S) is a kind of secondary mineral formed by oxidation, reduction, dissemination, and migration of primary sulfides such as chalcopyrite. As an important raw material for copper extraction, chalcocite has the highest copper content in copper sulfide minerals. Bioleaching of chalcocite has the advantages of economy and environmental protection. Its principle is to complete the oxidation of Fe^{2+} and S^{2-} by bacteria and directly or indirectly promote the dissolution of copper sulfide minerals.[1] With the gradual depletion of chalcopyrite-dominant copper ores, more and more chalcocite-dominant copper ores with a high pyrite content are treated. However, in the middle and later periods of bioleaching of copper ores, iron ions in the leaching solution tend to accumulate rapidly.[2] This problem increases the difficulty of separating copper and iron ions from the leaching solution and makes the influence of wastewater on the environment deeper. Therefore, it is necessary to selectively dissolve chalcocite from the secondary sulfide copper ores with a high pyrite content in bioleaching.

In chalcocite-dominant copper ores, Fe mainly exists as pyrite (FeS_2). In bioleaching, S^{2-} on the surface of pyrite participates in the single electron transfer reaction, and is oxidized to S_n^{2-}, S^0, and SO_4^{2-} in turn by bacteria.[3] Fe^{2+} is oxidized to Fe^{3+} by bacteria and entered the solution to promote the dissolution of chalcocite.[4] Chalcocite is transformed into covellite by multistep oxidation. Under the action of Fe^{3+} and dissolved oxygen, covellite is further decomposed into Cu^{2+} and S^0.[5] Obviously, Fe^{2+} ions produced by pyrite dissolution are closely related to the dissolution of chalcocite, and are also the main source of Fe^{2+} ions required by bacteria.

Previous studies have shown that dissolved oxygen and Fe^{3+} are the two main oxidants for pyrite dissolution. With the low pH value, the oxidation rate of pyrite is positively correlated with the concentration of Fe^{3+}.[6,7] Because the change of the concentration ratio between Fe^{3+} and Fe^{2+} determined the oxidation reduction potential (ORP), the dissolution rate of pyrite is closely related to the solution potential. Electron transfer of the oxidant from the mineral surface to the solution is a limited step in pyrite dissolution. Therefore, the oxidation of pyrite is controlled by the chemical reaction.[8] When the solution potential is greater than 546 mV in bioleaching, the bonds on the surface of pyrite break and the ore begin to dissolve.[9] When the solution potential is greater than 600 mV, the oxidation rate of pyrite accelerated significantly,[10] and bacteria can increase the oxidation rate of Fe^{2+} by more than

Received: July 23, 2019
Accepted: August 21, 2019
Published: October 22, 2019

DOI: 10.1021/acsomega.9b02294
ACS Omega 2019, 4, 18279−18288

Table 1. Chemical Composition Analysis of Sample

element	Cu	S	Fe_2O_3	As	SiO_2	Al_2O_3	CaO	K_2O	Na_2O	MgO
content (wt %)	0.28	3.51	3.03	0.02	78.77	14.17	0.07	1.48	0.06	0.05

10^6 times.[11] Therefore, it can be considered that controlling bacterial activity and delaying the oxidation of Fe^{2+} are the two essential methods to control pyrite dissolution. Previous studies have shown that the bioleaching of chalcocite is controlled by the diffusion of Fe^{3+} ions and chemical reactions. When the concentration of Fe^{3+} in the solution is lower than 0.058 mol/L, the leaching process is mainly controlled by the mass transfer of Fe^{3+} ions. When the concentration of Fe^{3+} ions is higher than 0.058 mol/L, the leaching process is mainly controlled by the surface charge transfer of minerals.[12] Compared with pyrite, the leaching of chalcocite is less affected by bacteria. With the increase of the Cu^{2+} concentration in the solution, the number of bacteria on the surface of chalcocite decrease, and Cu^{+} are mainly oxidized by Fe^{3+} in the solution.[13,14] At present, the dissolution behavior of pyrite in bioleaching has been studied extensively. However, more theoretical analyses about the dissolution characteristics of mixed minerals containing pyrite and chalcocite are needed.

The surface reaction of a metal sulfide semiconductor in an electrolyte solution is the critical factor affecting its dissolution mechanism. The difference between the ORP of the solution and the Fermi level of the solid determines the reaction mechanism. The semiconductor band model can describe the reaction process of the sulfide ore surface in the solution clearly. Holmes and Crundwell have explained the dissolution mechanism of pyrite in acidic solution by energy band diagram.[7] The diagram shows the energy levels of solid and liquid at the pyrite−solution interface. At the dissolution equilibrium, the Fermi levels of solids and liquids are equal. The study on the mixed bioleaching system of sphalerite, pyrite, and chalcopyrite shows that bacteria enhance copper leaching mainly by enhancing the ability of oxygen to obtain electrons.[15] Obviously, the model of the energy band can also be used to explain the dissolution mechanism of chalcocite in the presence of pyrite in bioleaching.

Using the first-principles method of density functional theory (DFT), we can accurately obtain the crystal parameters and properties of various minerals. This provides great convenience for the theoretical analysis of the energy band in the dissolution of sulfide ores. However, there are few DFT studies and band analyses in bioleaching of chalcocite, which have significant research value. Based on the analysis of previous works, we speculate that the dissolution of chalcocite in real minerals is easier on the conditions of higher solution potential and the ferrous oxidation rate. In this paper, pure minerals of chalcocite and pyrite were separated from secondary copper sulfide samples. By analyzing the change of the solution potential and the bacterial community structure, the difference of dissolution of two minerals in bioleaching was studied. Subsequently, the crystal models of chalcocite and pyrite were constructed, and the energy band distributions of the two minerals in real conditions were investigated. Our objectives are to determine the dominant group in the selective leaching and the leaching effect of chalcocite with the change of the solution potential and the bacterial community structure. Furthermore, the role of pyrite in selective bioleaching of real minerals should also be determined to explain the mechanism of selective dissolution of chalcocite in bioleaching.

2. RESULTS AND DISCUSSION

2.1. Effect of Bacteria on the Leaching Process of Pure Minerals. The chemical composition analysis results of the secondary copper sulfide sample are shown in Table 1. It shows that the sample contained 0.28% of Cu, 3.03% of Fe, and 3.51% of S, respectively. The sample consists of quartz, muscovite, pyrite, chalcocite, and a small amount of covellite, as described in the previous work.[35] It can be inferred that copper mainly exists in the form of chalcocite and covellite, and iron mainly exists in the form of pyrite.

Table 2 shows the chemical composition analysis results of two pure minerals separated and enriched from the raw ore. It shows that the purity of the two pure mineral samples is greater than 92%. The content of Fe in chalcocite and Cu in pyrite is less than 3%, which means that the influence of the two elements on the dissolution of respective main minerals can be neglected.

Table 2. Chemical Composition Analysis of Pure Minerals (wt %)

mineral	Cu	Fe	S	SiO_2	purity
chalcocite	68.42	2.53	23.98	0.11	92.40
chalcocite (theoretical)	80.00		20.00		100.00
pyrite	0.19	44.19	47.94	1.39	92.13
pyrite (theoretical)		46.67	53.33		100.00

The leaching experiments of pure minerals were carried out in conical flasks. The effect of the inoculation ratio on the leaching efficiency of metal ions from two pure minerals was investigated. The results are shown in Figure 1.

As shown in Figure 1, the leaching effects of metal ions from chalcocite and pyrite by bacteria are obviously different. Between 0 and 120 h, the leaching efficiency of Cu increases slowly. When the leaching time exceeded 120 h, the leaching efficiency increases significantly. For pyrite, the increase of leaching efficiency of Fe is the highest from 75 to 220 h. After

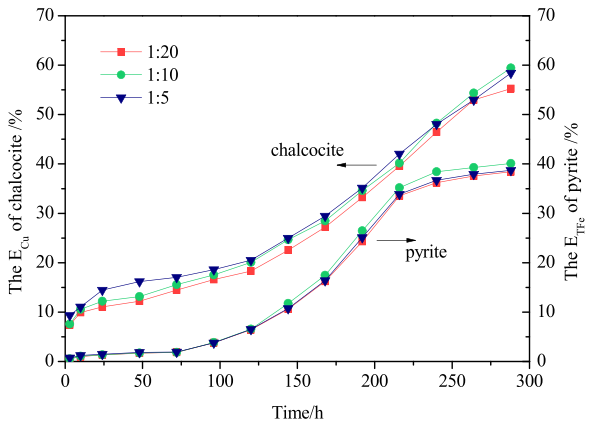

Figure 1. Effect of various inoculation ratios (1:20, 1:10, and 1:5) on leaching efficiency of pure minerals at 30 °C.

DOI: 10.1021/acsomega.9b02294
ACS Omega 2019, 4, 18279−18288

220 h, the leaching efficiency of Fe barely changes. At the same leaching moment, the leaching efficiency of Cu is always higher than pyrite. It can be seen that the change of the inoculation ratio has little effect on the leaching efficiency of metal ions from two pure minerals. The results show that the leaching efficiency of Cu is higher when the inoculation ratio is 1:10.

The solution potential was controlled during the leaching process. The dissolution differences of the two pure minerals at solution potentials of 640 mV and 800 mV were investigated. The results are shown in Figures 2 and 3.

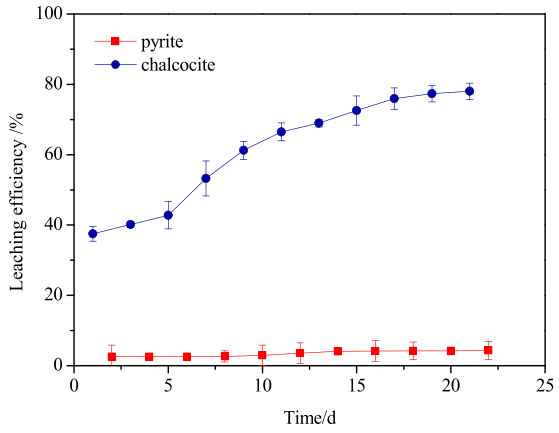

Figure 2. Leaching efficiency variety of chalcocite and pyrite with time at 640 mV of solution potential and 30 °C (the initial pH value is 1.8).

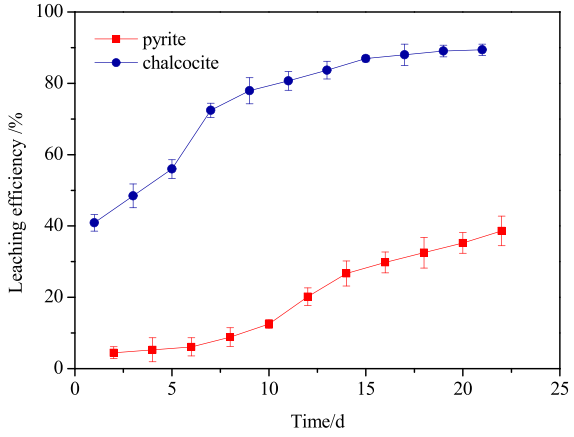

Figure 3. Leaching efficiency variety of chalcocite and pyrite with time at 800 mV of solution potential and 30 °C (the initial pH value is 1.8).

As shown in Figures 2 and 3, with the change of the solution potential, the leaching efficiencies of copper and iron ions are different obviously. Changes of potential have little effect on the dissolution of chalcocite. At 640 mV of solution potential, the leaching efficiency of Cu is more than 75%, while the leaching efficiency of Fe is only about 5% on day 20. At 800 mV of solution potential, the leaching efficiency of Cu is close to 90%, and the leaching efficiency of Fe increased above 40%. It can be inferred that the solution potential has a significant effect on the selective leaching of chalcocite. A lower solution potential is helpful for selective dissolution of chalcocite.

2.2. Effect of Bacteria on Leaching Process of Mixed Pure Minerals. Due to the existence of Fe^{3+}/Fe^{2+} pairs, Fe^{3+} in the solution can simultaneously promote the oxidation of Cu^{+} in chalcocite and Fe^{2+} in pyrite, and promote the dissolution of the two minerals in the leaching system. The ratio of Fe^{3+}/Fe^{2+} pair will be affected by the release of Fe^{2+} from pyrite dissolution, and the potential of the solution will be affected. Therefore, it is helpful to understand the selective leaching mechanism of chalcocite by mixing pure minerals of pyrite and chalcocite and studying the leaching characteristics of the mixed ore.

The chalcocite/pyrite mixed pure minerals with a mass ratio of 1:2 were leached at 30 °C for 14 days. The variation of metal ion leaching efficiency and solution potential with time is shown in Figures 4 and 5.

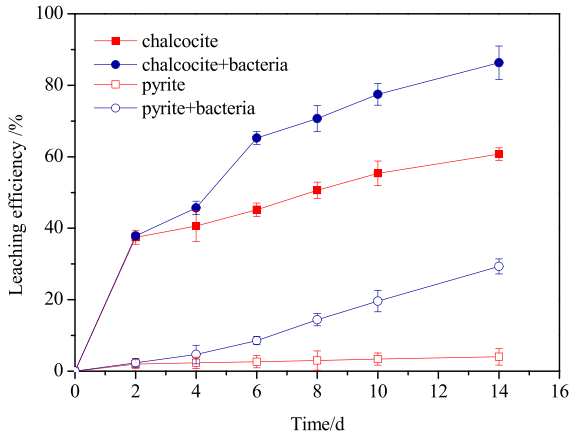

Figure 4. Leaching efficiency variety of chalcocite and pyrite with time (the initial pH value is 1.8 and the inoculation ratio is 1:10).

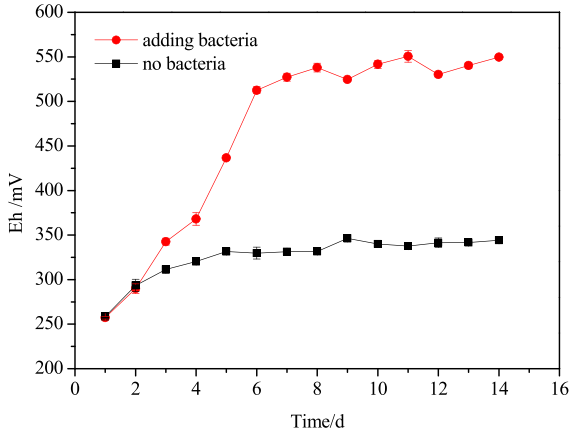

Figure 5. Solution potential variety of mixed pure minerals with time.

It can be seen from Figure 4 that the presence of bacteria has different effects on the leaching efficiency of copper and iron from mixed pure minerals. When there were no bacteria in leaching, because of the higher electrostatic potential of pyrite, the contact between pyrite and chalcocite would produce a galvanic effect, which would inhibit the dissolution process of pyrite as the cathode.[21] The dissolution of pyrite and chalcocite was promoted after bacterial inoculation. With the presence of bacteria, the potential of the solution increases from 260 mV to about 550 mV after 14 days of bioleaching (Figure 5). This indicates that the oxidation of Fe^{2+} in the solution and mineral surface by bacteria increases the potential of the solution, accelerates the mineral dissolution rate, and

DOI: 10.1021/acsomega.9b02294
ACS Omega 2019, 4, 18279−18288

then increases the difference of leaching efficiency between two sulfide ores due to the galvanic effect.

Therefore, bacteria can promote the dissolution of mixed pure minerals, and the selective dissolution of chalcocite can be achieved by controlling the potential of the solution.

2.3. Varieties of Microbial Community Structures during Selective Leaching. *2.3.1. Response of Microbial Community Structures on Different Sulfide Minerals.* The structures of the microbial community absorbed on the leached sample of different sulfide ores were analyzed by the sequencing strategy PE300. The results are shown in Figure 6. Original represents the starting strain. Pyrite and chalcocite represent the microbial communities in the leaching solution of the two pure minerals, respectively.

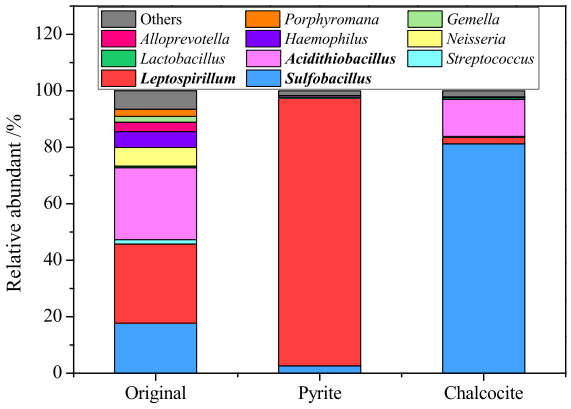

Figure 6. Frequency of genus in microbial communities from bioleaching solution of pure minerals after 14 days of bioleaching (original represents the starting strain).

The results in Figure 6 show that the dominant genera in the starting strain are classified into *Leptospirillum*, *Acidithiobacillus*, and *Sulfobacillus*, which have strong oxidation ability toward iron and sulfur. *Leptospirillum* is the dominant bacterium in pyrite leaching, while *Acidithiobacillus* and *Sulfobacillus* are the dominant bacteria in chalcocite leaching. The proportion of *Sulfobacillus* is higher. It can be inferred that the dissolution of pyrite is mainly promoted by the oxidation of low-valent iron by *Leptospirillum*, while the dissolution of chalcocite is mainly promoted by the oxidation of low-valent sulfur by *Acidithiobacillus* and *Sulfobacillus*.

2.3.2. Response of the Community Succession on Solution Potential. The leaching experiments of secondary copper sulfide samples were carried out in a stirred tank reactor. The effect of the solution potential on the leaching efficiency of Cu from copper sulfide ore samples was investigated. The results are shown in Figure 7.

The initial solution potential is 370 mV. Figure 7 shows that the Cu in the sample has obvious selective dissolution characteristics when the solution potential is controlled. When the solution potential is greater than 700 mV, the Cu leaching efficiency is greater than 75%, while the Fe leaching efficiency is only about 6%. Although the Cu leaching efficiency reached about 80% above 700 mV, the Fe leaching efficiency rapidly increased to more than 30%. Therefore, the selective leaching of chalcocite is effective when the solution potential is controlled below 700 mV.

The structure of the microbial community absorbed on the leached sample at different solution potentials was analyzed by

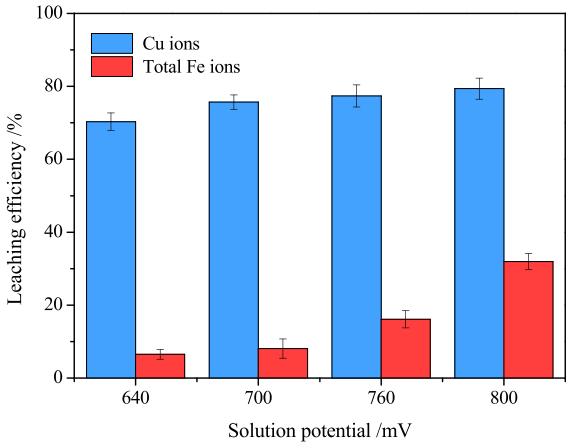

Figure 7. Leaching efficiency variety of Cu and Fe ions with solution potential after 14 days (the initial pH value is 1.8 and the inoculation ratio is 1:10).

the sequencing strategy PE300. The results are shown in Figure 8. Samples are represented by numbers 1−6. The

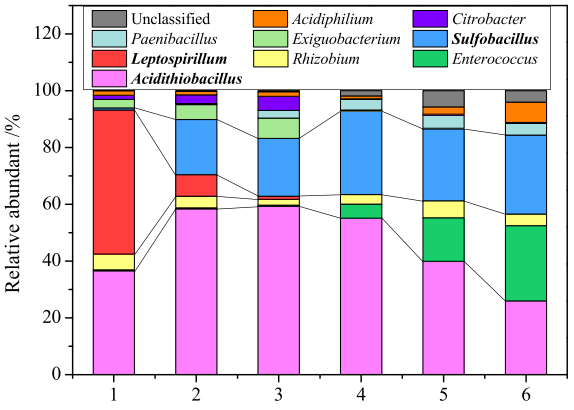

Figure 8. Frequency of genus in microbial communities of copper sulfide ores at different potentials after 14 days of bioleaching (1−6 represent the samples from different potential control conditions).

potential of sample 1 is not controlled during leaching, and the potential is higher than 840 mV. The solution potential of samples 2−6 are controlled to be 800, 760, 700, 640, and 600 mV, respectively.

As shown in Figure 8, the structures of microbial communities change greatly at different potentials. At 840 mV, the dominant bacteria is mainly *Leptospirillum*, whose proportion decreases rapidly at lower potential. It was reported that *Leptospirillum ferriphilum* was the dominant iron(II)-oxidizer in later stages of leaching.[22,23] At 700 mV or a lower potential, the proportion of *Leptospirillum* decreases to almost 0, and is mainly replaced by *Acidithiobacillus* and *Sulfobacillus*.

It can be inferred that the iron oxidizing ability of the community dominated by *Leptospirillum* at high potential is stronger. The increased dissolution rate of pyrite leads to more iron ions and is not conducive to the extraction and separation of copper from the leaching solution. Conversely, the sulfur oxidation ability of the community dominated by *Acidithiobacillus* and *Sulfobacillus* at low potential is stronger. The two bacteria are conducive to the selective dissolution of chalcocite. It was reported that in pyrite bioleaching of *Acidithiobacillus*, the thiosulfate leads to sulfate without S

DOI: 10.1021/acsomega.9b02294
ACS Omega 2019, 4, 18279−18288

formation.[24] Obviously, the presence of sulfur-oxidizing bacteria also eliminates the effect of sulfur in leaching.

2.4. Semiconductor Band Theory Analysis of Selective Leaching of Chalcocite. Based on the density functional theory, the crystal models of chalcocite and pyrite were constructed using the program CASTEP. Structural optimizations and electronic property calculations were also performed. The crystal structures is shown in Figure 9. There are Fe−S bonds and S−S bonds in the pyrite cell, and only Cu−S bonds and Cu−Cu bonds in the chalcocite cell.

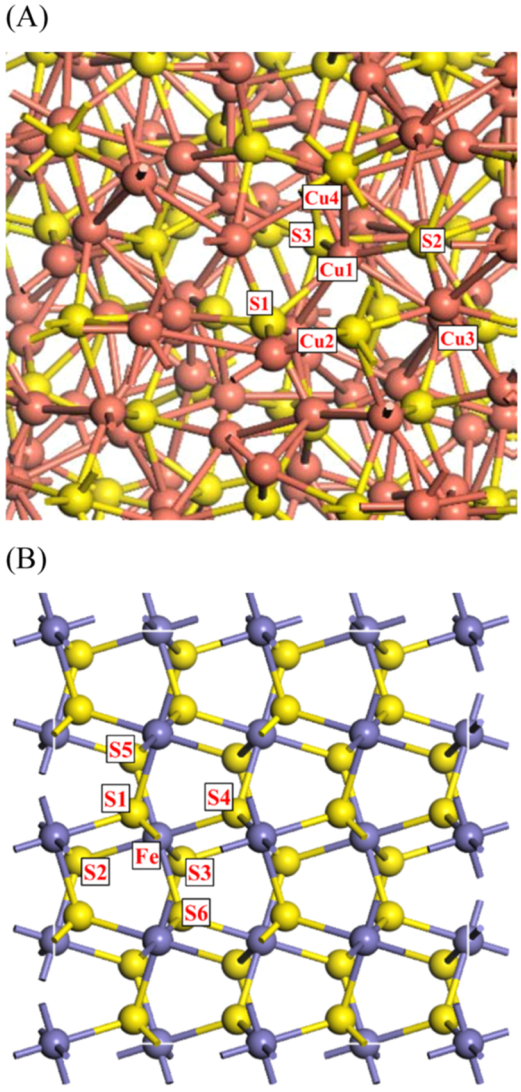

Figure 9. Coordination of Fe and Cu atoms in chalcocite and pyrite. (A) chalcocite; (B) pyrite.

2.4.1. Analysis of Mulliken Population. Mulliken population is a method proposed to show the distribution and bonding of electric charges between constituent atoms, which characterizes the distribution, transfer, and bonding properties of electrons between atoms. When the population is greater, the covalent bonds formed between the atoms are stronger. Conversely, for a smaller population, electron clouds have a small degree of overlap and the bond exhibits ionicity. The atomic coordination of the two minerals are shown in Figure 9. Mulliken population analysis focuses on bonds formed by atoms around vacancies. The populations of ideal and defective pyrite and chalcocite are listed in Tables 3 and 4.

Table 3. Mulliken Population of Ideal and Defective Pyrite

	bond	length (Å)	population
ideal crystal	Fe−S	2.241	0.48
	S−S	2.178	0.31
Fe vacancy	Fe−S1	2.246	0.47
	Fe−S2	2.240	0.48
	Fe−S3	2.268	0.43
	Fe−S4	2.254	0.47
	Fe−S5	2.203	0.50
	Fe−S6	2.235	0.48
	S−S	2.188	0.32
S vacancy	Fe−S1	2.242	0.48
	Fe−S2	2.233	0.48
	Fe−S3	2.239	0.47
	Fe−S4	2.241	0.47
	Fe−S5	2.242	0.48
	Fe−S6	2.248	0.48
	S−S	2.175	0.35

Table 4. Mulliken Population of Ideal and Defective Chalcocite

	bond	length (Å)	population
ideal crystal	Cu1−Cu2	2.687	0.05
	Cu1−S1	2.288	0.40
	Cu1−S2	2.340	0.40
	Cu1−Cu3	2.683	0.70
	Cu1−S3	2.406	0.30
	Cu1−Cu4	2.609	0.16
Cu vacancy	Cu1−Cu2	2.742	0.05
	Cu1−S1	2.522	0.18
	Cu1−S2	2.684	0.09
	Cu1−Cu3	2.244	0.45
	Cu1−S3	2.649	0.12
	Cu1−Cu4	2.318	0.39
S vacancy	Cu1−Cu2	2.723	0.04
	Cu1−S1	2.448	0.24
	Cu1−S2	2.639	0.12
	Cu1−Cu3	2.227	0.52
	Cu1−S3	2.672	0.12
	Cu1−Cu4	2.352	0.33

In Table 3, with the presence of Fe vacancy in the pyrite crystal, the length of most Fe−S bonds increases slightly, the population decreases from 0.48 to 0.43, and the bonds covalency are stronger. The length of the S−S bond increases slightly with a little change of the population. In the pyrite crystal with S vacancy, the lengths of most Fe−S bonds increase slightly and the populations remain unchanged. The length of the S−S bond decreases slightly, while the population increases from 0.31 to 0.35, and the bond covalency is also stronger. The above results show that the surface of pyrite with Fe vacancy has stronger hydrophilicity than ideal pyrite.[18] The presence of vacancy enhances the atomic activity in the Fe−S bond, and reduce the reaction difficulty between pyrite and electron acceptors such as O_2 and Fe^{3+} in the solution. The presence of S vacancy mainly weakens the activity of S atoms in S−S bonds and increases the reaction difficulty between pyrite and electron acceptors in the solution.

DOI: 10.1021/acsomega.9b02294
ACS Omega 2019, 4, 18279−18288

In Table 4, with the presence of Cu vacancy in the chalcocite crystal, the lengths of Cu−S bonds decrease significantly, the populations decrease from 0.30−0.40 to 0.09−0.18, and the bond ionicity becomes stronger. In the chalcocite crystal with S vacancy, the populations of Cu−S bonds decrease to 0.12, with a stronger bond ionicity. The length and population of Cu−Cu bonds in chalcocite with vacancy have no directional variation trend. The above results show that the surface of chalcocite with Cu or S vacancy has stronger hydrophilicity than ideal chalcocite. The presence of vacancies enhances the atomic activity in Cu−S bonds and reduces the reaction difficulty between chalcocite and electron acceptors in the solution. It is difficult to bond between S atoms in chalcocite.

2.4.2. Analysis of Density of States (DOS). The band structure and atomic density of states (DOS) of two mineral cells are shown in Figures 10 and 11. The value of the Fermi level is set at 0 eV.

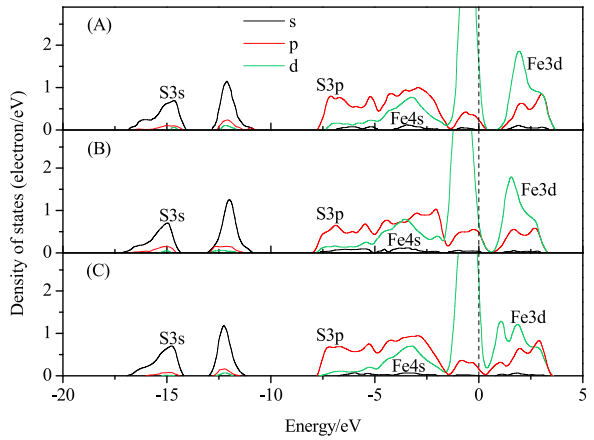

Figure 10. DOS of atoms on different types of pyrite. (A) ideal crystal; (B) Fe vacancy crystal; (C) S vacancy crystal.

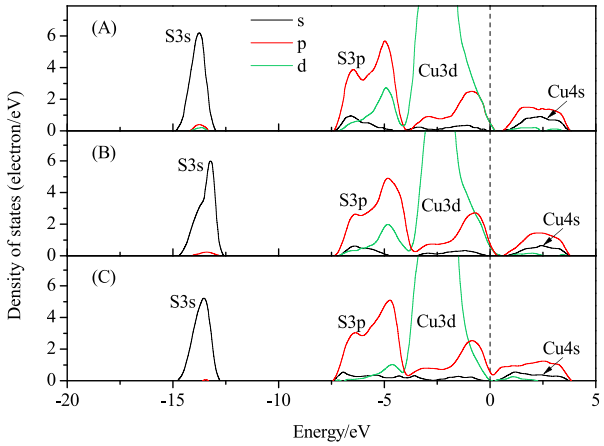

Figure 11. DOS of atoms on different types of chalcocite. (A) ideal crystal; (B) Fe vacancy crystal; (C) S vacancy crystal.

In Figures 10 and 11, the DOS at the Fermi level is close to 0. Therefore, the crystals mainly exhibit semiconductor properties. As shown in Figure 10, the valence band of pyrite from −17 to −10 eV is mainly contributed by the S 3s orbital, followed by the Fe 3d, Fe 4s, and S 3p orbitals, and the Fe 4p orbit has the least contribution. The energy range from −8.0 to −1.5 eV below the top of the valence band is mainly contributed by Fe 4s and S 3p orbitals. Among them, S 3p orbital contributes more, followed by the Fe 4s orbital. The Fe 3d orbital in the valence band near the Fermi level contributes more and the activity of Fe atoms are stronger. With the presence of Fe and S vacancies, the DOS of pyrite from 0.4 to 3.5 eV is less than ideal pyrite, and the atomic activity of Fe increases, which is consistent with the results of Mulliken population analysis. S vacancy also leads to an increase of DOS at the Fermi level and a decrease of the energy gap, which enhances the metallicity of pyrite.

As shown in Figure 11, the valence band of chalcocite from −15 to −13 eV is mainly contributed by the S 3s orbital, followed by the S 3p orbital. The energy range from −7.0 to 0 eV below the top of the valence band is mainly contributed by Cu 3d and S 3p orbitals. The Cu 3d orbital in the valence band near the Fermi level contributes more and the activity of the Cu atoms are stronger. With the presence of Cu and S vacancies, the DOS of chalcocite from −7.5 to 0.5 eV is less than ideal chalcocite, and the atomic activity of Cu and S increases. The Cu and S vacancies in chalcocite lead to a decrease of the bond energy of copper and S from −7.5 to 0.5 eV, and an increase of the activity of copper and S atoms. The S vacancy also leads to an increase of DOS and a decrease of the energy gap at the Fermi level. S vacancy also leads to an increase of DOS at the Fermi level and a decrease of the energy gap.

2.4.3. Analysis of Band Theory in Selective Dissolution of Chalcocite. Previous studies showed that at the higher Fermi level than the ORP of the solution, the electrons would migrate from the semiconductor to the solution and the electron-deficient region would be formed on the semiconductor surface.[25,26] The Fermi levels of chalcocite and pyrite were calculated by Dmol^3. The results are shown in Table 5.

Table 5. Calculated Value of Fermi Levels of Chalcocite and Pyrite

minerals	the calculated value (eV)
pyrite (ideal)	−5.690
pyrite (Fe vacancy)	−5.638
pyrite (S vacancy)	−5.621
chalcocite (ideal)	−4.555
chalcocite (Cu vacancy)	−4.539
chalcocite (S vacancy)	−4.446

As shown in Table 5, the Fermi levels of ideal chalcocite and ideal pyrite are −4.56 eV and −5.69 eV, respectively. Fe, Cu, and S vacancies raise the Fermi level of chalcocite and pyrite. The increase of the Fermi level is beneficial to the transfer of electrons from the mineral surface to the solution, and to the adsorption of dissolved oxygen on the surface. With the increase of the hole on the surface, S^{2-} and S are more easily oxidized to SO_4^{2-}. This causes the formation of more hydrophilic groups on the surface of the two sulfide ores and the acceleration of mineral dissolution. No matter what vacancy exists, there are significant differences between the Fermi levels of the two minerals. The band gap width of pyrite is about 0.95 eV, while that of chalcocite is about 1.1 eV.[27,28] Based on the Fermi level data in Table 5, the schematic diagrams of the energy band structure of chalcocite and pyrite are drawn in Figure 12.

In semiconductor physics, the energy level of the standard hydrogen electrode (SHE) can be determined to be −4.5 eV.

DOI: 10.1021/acsomega.9b02294
ACS Omega 2019, 4, 18279−18288

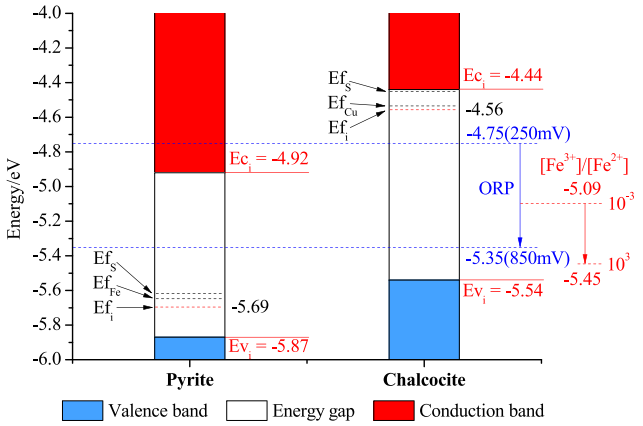

Figure 12. Energy band structure of chalcocite and pyrite including the solution energy level. E_F, E_c, and E_v represent Fermi energy, valence band maximum, and conduction band minimum, respectively. The subscripts Fe, S, and i represent Fe vacancy, S vacancy, and ideal crystal, respectively.

The relationship between energy level E and solution potential E_h can be expressed by eq 1.[29]

$$E(\mathrm{eV}) = -E_h(\mathrm{V}) - 4.5 \quad (1)$$

In bioleaching, the solution potential fluctuates in the range of 250−850 mV (vs SHE). The energy level corresponding to the potential is between the Fermi level of chalcocite and pyrite. According to the Nernst equation, when the ratio of Fe^{3+}/Fe^{2+} changes from 10^{-3} to 10^{3}, the corresponding energy levels of potential change from −5.45 to −5.09 eV. The energy levels of the solution and Fe^{3+}/Fe^{2+} pairs are also shown in Figure 12.

Figure 12 shows that the Fermi level of ideal pyrite (−5.69 eV) is lower than the energy level of the solution (−4.75 to −5.35 eV) without adding bacteria. Electrons can migrate from the solution to the pyrite surface and form an electron accumulation zone. At a lower solution potential (Figure 5, about 330 mV), the energy difference between the top of the pyrite valence band and the solution (about 1.04 eV) is greater than the width of the pyrite gap (0.95 eV). Therefore, it is difficult to form electron holes at the top of the valence band, and the apparent dissolution rate of pyrite is relatively low (Figure 4). The Fermi level (−4.56 eV) of ideal chalcocite is greater than the energy level of the solution. Electrons can easily migrate from the chalcocite surface to the solution. The formation of more holes on the surface of chalcocite promotes the fracture of the Cu−S bond, which shows a higher apparent dissolution rate (Figure 4).

Fermi levels of pyrite and chalcocite increase with the presence of vacancies in both crystals. For pyrite, it is easier to form holes on the Fe−S bond and the dissolution rate of pyrite increases. For chalcocite, the rate of electron migration from the Cu−S bond to the solution accelerates. Chalcocite tends to further transform into covellite and dissolve.

With the presence of bacteria, *Acidithiobacillus* and *Sulfobacillus* oxidize low-valent sulfur to S^0, $S_2O_3^{2-}$, and SO_4^{2-} and assist the oxidation of Fe^{2+}, which increases the ratio of Fe^{3+}/Fe^{2+} and the solution potential. When the energy level of the solution crosses the bottom energy level of the ideal pyrite conduction band (−4.92 eV) and approaches the top energy level of the valence band (−5.87 eV), the electron holes at the top of the valence band increase, and the dissolution rate of pyrite also increases. At the same time, the loss of electrons at the top of the ideal chalcocite valence band brings a large number of holes. Cu^+, which moves to the solid−liquid interface continuously is oxidized to Cu^{2+} by dissolved oxygen and Fe^{3+} of the solution. When the potential is not controlled, the concentration of Fe^{3+} and the potential of the solution will continue to increase. Above 800 mV, *Leptospirillum* becomes a dominant group, rapidly oxidizing Fe^{2+} and leads to the increase of the Fe^{3+}/Fe^{2+} ratio continuously. It is difficult to inhibit the dissolution of pyrite.

If vacancies exist in pyrite and chalcocite crystals, *Leptospirillum* will replace *Acidithiobacillus* and *Sulfobacillus* as the dominant group earlier because of the higher Fe^{2+} concentration in the solution.

If the potential of the solution is controlled at a lower level (<700 mV or −5.2 eV), the oxidation extent of Fe^{2+} by *Leptospirillum* is limited, and the concentration of Fe^{3+} in the solution is relatively low. Chalcocite is selectively dissolved by oxygen and a small amount of Fe^{3+} in the solution. Because of the presence of Fe, Cu, and S vacancies, the Fermi level of real minerals is higher than ideal. Therefore, the solution potential should be controlled at 600 mV or less to ensure the selective dissolution of chalcocite.

Accordingly, we can consider the feasibility of treating the secondary sulfide ore by two-stage bioleaching. In the first stage of bioleaching, ORP is maintained below 600 mV, so that chalcocite is completely converted to covellite and some copper ions, and the iron leaching amount is controlled at a low level. In the second stage, the separation of covellite and pyrite is considered to realize the effective control of the iron ion concentration in the leaching solution. The kinetic investigation of the two-stage dissolution process of chalcocite also supports this view indirectly.[30]

3. CONCLUSIONS

Through bioleaching and first-principles method analysis of secondary copper ores and pure minerals, the mechanism of selective dissolution of chalcocite in bioleaching was explained.

For pure minerals, the leaching efficiency of copper from chalcocite was higher than pyrite at the same leaching time. Controlling the solution potential at a lower level was beneficial to the selective leaching of chalcocite. For mixed pure mineral, bacteria increased the leaching efficiency of metal ions from pyrite and chalcocite simultaneously by oxidizing Fe^{2+} to Fe^{3+} in the solution.

Acidithiobacillus and *Sulfobacillus* were the dominant group in the leaching of chalcocite, and the proportion of *Sulfobacillus* was higher. *Leptospirillum* was the dominant bacterium in the leaching of pyrite. Below 700 mV of solution potential, the bacterial community, mainly consisted of *Acidithiobacillus* and *Sulfobacillus*, had a stronger promotion on the selective dissolution of chalcocite.

In bioleaching, the solution energy level was higher than ideal pyrite but lower than ideal chalcocite, which resulted in the accumulation of electrons on the surface of pyrite and the formation of holes at the top of the chalcocite valence band. When bacteria assisted the oxidation of Fe^{2+} to Fe^{3+} and caused the raise of the solution potential, the difference between the solution energy level and the top of the pyrite valence band would be smaller than the width of the pyrite energy gap. Then, the holes at the top of the pyrite valence band increased. The acceleration of pyrite dissolution provided more Fe^{2+} for *Leptospirillum*. Below 700 mV, the assistances of *Acidithiobacillus* and *Sulfobacillus* on the oxidation of Fe^{2+} were

DOI: 10.1021/acsomega.9b02294
ACS Omega 2019, 4, 18279−18288

weak, and the concentration of Fe^{3+} was relatively low. Chalcocite was selectively dissolved by oxygen and a small amount of Fe^{3+} in the solution.

Because of the presence of Fe, Cu, and S vacancies in real minerals, the surface of chalcocite and pyrite had stronger hydrophilicity than ideal minerals. The atomic activity in the Cu−S bond and the Fe−S bond enhanced, and the reaction difficulty between minerals and electron acceptors in the solution reduced. Real minerals had smaller energy gaps and higher Fermi levels. *Leptospirillum* could replace *Acidithiobacillus* and *Sulfobacillus* as the dominant group at 600 mV or more. Therefore, the solution potential should be controlled at a lower level to ensure the selective dissolution of chalcocite.

4. MATERIALS AND METHODS

4.1. Samples. The secondary copper sulfide sample was obtained from the Zijinshan Copper Mine of Fujian Province of China. The particle size of the sample was less than 2 mm. Pure minerals of pyrite and chalcocite were obtained by separating and enriching from raw ore through hand sorting, gravity separation, and flotation. Pure minerals were all ground and sieved to minus 0.074 mm.

The bacteria used in the experiment were collected from the sump pit of ore heap of Zijinshan Copper Mine. After 4 to 5 days' breeding and domestication in the laboratory, the bacteria with good tolerance on copper and iron ions were obtained. Bacteria were cultured on 9 K medium. The optimum growth temperature of the bacteria is 30−45 °C, and the optimum pH value is about 1.2−2.5.

4.2. Leaching Experiments. The copper sulfide sample and pure minerals were ground and sieved to minus 0.074 mm, respectively. The leaching experiments of pure minerals were carried out in conical flasks. A certain amount of samples and 9 K medium were added into the conical flask. The pH of the solution was adjusted to a certain value between 1.8 and 2.0 with 20% (v/v) sulfuric acid and ensured that the initial pH of the solution in the conical flasks was the same so that the initial solution potential was roughly the same. The initial inoculated cell density was 2×10^7 cells/mL. The inoculation ratio (volume ratio of bacterial liquid to pulp) in conical flasks were 1:20, 1:10, and 1:5, respectively. In the process of leaching, the pH and potential of the solution were measured every day, and the concentration of copper and iron ions in the supernatant were measured every 3 days. After leaching, residues were filtered and dried. The leaching experiments of copper sulfide samples were carried out in a stirred tank reactor, as shown in Figure 13. The reactor could detect the solution pH value and ORP online and control the potential by filling different gases during the leaching process. Before every leaching, the pulp concentration was adjusted to 5%. In the leaching process, the stirring speed was 120 rpm, and the temperature was controlled in the range of 30−35 °C. The pH range of the solution was the same as that of pure mineral leaching experiment. After leaching, residues were filtered and dried.

4.3. Model of Crystal Structures of Minerals. Based on the density functional theory, the calculations were performed using the programs CASTEP and DMol^3. Structural optimizations and electronic property calculations were performed using CASTEP and GGA-PW91.[16,17] The valence electrons (Fe $3d^64s^2$, S $3s^23p^4$, and Cu $3d^{10}4s^2$) were considered using ultra-soft pseudopotentials.[18] A plane wave basis set with an energy cutoff of 270 eV was employed for the geometry optimization. A Monkhorst−Pack *k*-point sampling

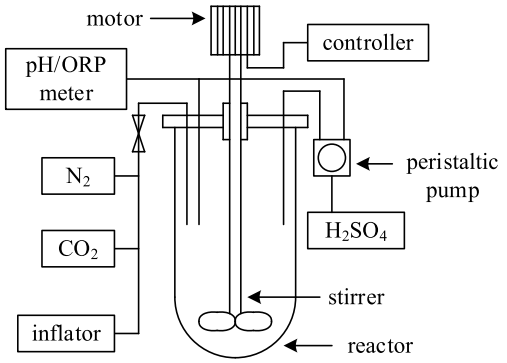

Figure 13. Stirred tank reactor with the function of detecting and controlling the pH and potential of the solution.

density of 2 × 2 × 2 mesh was used.[19,20] The convergence tolerances for geometry optimization calculations were set to the maximum displacement of 0.002 Å, the maximum force of 0.08 eV Å^{-1}, the maximum energy change of 2.0×10^{-5} eV/atom and the maximum stress of 0.1 GPa, and the self-consistent field (SCF) convergence tolerance was set to 2.0×10^{-6} eV/atom. The spin-polarization was used for all calculations. Properties were calculated with the same parameters as geometry optimization. The Fermi levels of crystals were calculated by Dmol^3, with the GGA-PW91 method, DNP basis set, effective core potentials, a fine quality, and SCF convergence threshold of 1.0×10^{-6} eV/atom.

4.4. Analytical Techniques. The chemical compositions were confirmed by X-ray fluorescence spectroscopy (XRF, XRF-1700, Shimadzu, Kyoto, Japan) using a standardless quantitative analysis method and chemical analyses. Microscopic observation and analysis of element distribution in leaching residues were conducted using a mineral liberation analyzer, which included a scanning electron microscope (JSM-7001F, Japan Electron Optics Laboratory, Tokyo, Japan) and an energy-dispersive X-ray fluorescence spectrometer (INCA X-Max, Oxford Instruments, Oxford, U.K.). Potential and pH of the leaching solution were determined by the pH/ORP meter (Seven Excellence S400, Mettler Toledo, Zurich, Switzerland) and a Pt electrode with reference to a Ag/AgCl electrode. All of the potential values mentioned were normalized to the hydrogen scale in this work. The concentrations of Cu^{2+} and total iron were determined by inductively coupled plasma optical emission spectrometry (725-Agilent Technologies, California).

The leaching efficiency E of metal ions were calculated by eq 2. In the equation, C is the concentration of metal ions, V is the volume of the solution, α is the grade of the metal, m is the mass of ore samples, and M is the molecular weight

$$E = 1 - \frac{C \times V \times M}{\alpha \times m} \times 100\% \quad (2)$$

Microorganisms were harvested from 5.0 mL representative leaching solutions. The cells were centrifuged at 12000*g* for 10 min for cell collection. Total DNA was extracted using the PowerWater DNA Isolation Kit (QIAGEN China Co. Ltd., Beijing, China). DNA quality assessment and quantification were conducted using a NanoDrop ND-1000 Spectrophotometer (NanoDrop Technologies Inc., Wilmington, DE). PCR was conducted on Applied Biosystems (ABI) Veriti 96-well Fast Thermal Cyclers with bacterial primer pair (341 F of the forward primer and 805 R of the reverse primer) for the

DOI: 10.1021/acsomega.9b02294
ACS Omega 2019, 4, 18279−18288

V3-V4 region of the 16 S rRNA gene.[31,32] Each sample was amplified under the following conditions: 94 °C for 5 min, 28 cycles at 94 °C for 45 s, 62 °C for 45 s, and 72 °C for 1 min, then 10 min at 72 °C. PCR products were purified using the EZNA Gel Extraction Kit (Omega Bio-tek). The library quality was assessed on the QuantiFluor-ST (Promega). Then, the library was sequenced on an Illumina Miseq platform (Majorbio, Shanghai) with the sequencing strategy PE300. The sequencing datasets of bacteria and fungi have been deposited in the National Center for Biotechnology Information (NCBI) Sequence Read Archive (SRA) (accession No. PRJNA555796).

4.5. Data Analysis. All sequence processing and diversity estimates were performed using the QIIME. To obtain clean tags, low-quality sequences and chimeras were filtered, trimmed, and removed.[33] Most of the sequence lengths after quality control were between 450 bp and 460 bp. High-quality nonchimeric sequences were clustered into operational taxonomic units (OTUs) using a 97% similarity threshold and the uclust algorithm with optimal uclust settings. The taxonomy of OTU representative sequences was phylogenetically assigned to taxonomic classifications by the RDP Classifier with a confidence threshold of 0.8.[34] All experiments were performed at least three times. Each data point and error bar represented the mean and standard deviation, respectively.

AUTHOR INFORMATION

Corresponding Author

*E-mail: yxl5071@163.com. Tel: +86 10 60662775.

ORCID

Xinlong Yang: 0000-0002-9035-638X

Notes

The authors declare no competing financial interest.

ACKNOWLEDGMENTS

This project was financially supported by the National Natural Science Foundation of China (No. 51574036).

REFERENCES

(1) Schippers, A.; Sand, W. Bacterial leaching of metal sulfide proceeds by two indirect mechanisms via thiosulfate or via polysulfides and sulfur. *Appl. Environ. Microbiol.* **1999**, *65*, 319−321.

(2) Jia, Y.; Tan, Q. Y.; Sun, H. Y.; Zhang, Y. P.; Gao, H. S.; Ruan, R. M. Sulfide mineral dissolution microbes: Community structure and function in industrial bioleaching heaps. *Green Energy Environ.* **2019**, *4*, 29−37.

(3) Fowler, T. A.; Holmes, P. R.; Crundwell, F. K. Mechanism of pyrite dissolution in the presence of *Thiobacillus ferrooxidans*. *Appl. Environ. Microbiol.* **1999**, *65*, 2987−2993.

(4) Lee, J.; Acar, S.; Doerr, D. L.; Brierley, J. A. Comparative bioleaching and mineralogy of composited sulfide ores containing enargite, covellite and chalcocite by mesophilic and thermophilic microorganisms. *Hydrometallurgy* **2011**, *105*, 213−221.

(5) Liu, H. C.; Xia, J. L.; Nie, Z. Y.; Wen, W.; Yang, Y.; Ma, C. Y.; Zheng, L.; Zhao, Y. D. Formation and evolution of secondary minerals during bioleaching of chalcopyrite by thermoacidophilic *Archaea acidianus* manzaensis. *Trans. Nonferrous Met. Soc. China* **2016**, *26*, 2485−2494.

(6) Bouffard, S. C.; Rivera-Vasquez, B. F.; Dixon, D. G. Leaching kinetics and stoichiometry of pyrite oxidation from a pyrite-marcasite concentrate in acid ferric sulfate media. *Hydrometallurgy* **2006**, *84*, 225−238.

(7) Holmes, P. R.; Crundwell, F. K. The kinetics of the oxidation of pyrite by ferric ions and dissolved oxygen: An electrochemical study. *Geochim. Cosmochim. Acta* **2000**, *64*, 263−274.

(8) Chandra, A. P.; Gerson, A. R. The mechanisms of pyrite oxidation and leaching: A fundamental perspective. *Surf. Sci. Rep.* **2010**, *65*, 293−315.

(9) Mikkelsen, D.; Kappler, U.; Webb, R. I.; Rasch, R.; McEwan, A. G.; Sly, L. I. Visualisation of pyrite leaching by selected thermophilic archaea: Nature of microorganism-ore interactions during bioleaching. *Hydrometallurgy* **2007**, *88*, 143−153.

(10) Cabral, T.; Ignatiadis, I. Mechanistic study of the pyrite−solution interface during the oxidative bacterial dissolution of pyrite (FeS_2) by using electrochemical. *Int. J. Miner. Process.* **2001**, *62*, 41−64.

(11) Gu, G. H.; Sun, X. J.; Hu, K. T.; Li, J. H.; Qiu, G. Z. Electrochemical oxidation behavior of pyrite bioleaching by *Acidithiobacillus ferrooxidans*. *Trans. Nonferrous Met. Soc. China* **2012**, *22*, 1250−1254.

(12) Angeles, C. Kinetics of Leaching of Covellite in Ferric-Sulfate-Sulfuric Acid Media. University of British Columbia: Vancouver, BC, 2015.

(13) Ruan, R. M.; Zhou, E.; Liu, X. Y.; Wu, B.; Zhou, G. Y.; Wen, J. K. Comparison on the leaching kinetics of chalcocite and pyrite with or without bacteria. *Rare Met.* **2010**, *29*, 552−556.

(14) Echeverría-Vega, A.; Demergasso, C. Copper resistance, motility and the mineral dissolution behavior were assessed as novel factors involved in bacterial adhesion in bioleaching. *Hydrometallurgy* **2015**, *157*, 107−115.

(15) Estrada-de los Santos, F.; Rivera-Santillán, R. E.; Talavera-Ortega, M.; Bautista, F. Catalytic and galvanic effects of pyrite on ferric leaching of sphalerite. *Hydrometallurgy* **2016**, *163*, 167−175.

(16) Segall, M. D.; Lindan, P. J. D.; Probert, M. J.; Pickard, C. J.; Hasnip, P. J.; Clark, S. J.; Payne, M. C. First-principles simulation: ideas, illustrated and the CASTEP code. *J. Phys.: Condens. Matter* **2002**, *14*, 2717−2744.

(17) Perdew, J. P.; Chevary, J. A.; Vosko, S. H.; Jackson, K. A.; Pederson, M. R.; Singh, D. J.; Fiolhais, C. Atoms, molecules, solids, and surfaces: Applications of the generalized gradient approximation for exchange and correlation. *Phys. Rev. B* **1992**, *46*, 6671−6687.

(18) Xi, P.; Shi, C. X.; Yan, P. K.; Liu, W. L.; Tang, L. G. DFT study on the influence of sulfur on the hydrophobicity of pyrite surfaces in the process of oxidation. *Appl. Surf. Sci.* **2019**, *466*, 964−969.

(19) Ahlberg, E.; Broo, A. E. Oxygen reduction at sulphide minerals. 2. A rotating ring disc electrode (RRDE) study at galena and pyrite in the presence of xanthate. *Int. J. Miner. Process.* **1996**, *47*, 33−47.

(20) Yakovkin, I. N.; Petrova, N. V. Influence of the thickness and surface composition on the electronic structure of FeS_2 layers. *Appl. Surf. Sci.* **2016**, *377*, 184−190.

(21) Wang, X. X.; Liao, R.; Zhao, H. B.; Hong, M. X.; et al. Synergetic effect of pyrite on strengthening bornite bioleaching by *Leptospirillum ferriphilum*. *Hydrometallurgy* **2018**, *176*, 9−16.

(22) Rawlings, D. E.; Coram, N. J.; Gardner, M. N.; Deane, S. M. *Thiobacillus caldus* and *Leptospirillum ferrooxidans* are widely distributed in continuous-flow biooxidation tanks used to treat a variety of metal-containing ores and concentrates. *Process Metall.* **1999**, *9*, 777−786.

(23) Mutch, L. A.; Watling, H. R.; Watkin, E. L. J. Microbial population dynamics of inoculated low-grade chalcopyrite bioleaching columns. *Hydrometallurgy* **2010**, *104*, 391−398.

(24) Liu, H.; Gu, G. H.; Xu, Y. B. Surface properties of pyrite in the course of bioleaching by pure culture of *Acidithiobacillus ferrooxidans* and a mixed culture of *Acidithiobacillus ferrooxidans* and *Acidithiobacillus thiooxidans*. *Hydrometallurgy* **2011**, *108*, 143−148.

(25) Bott, A. W. Electrochemistry of semiconductors. *Curr. Sep.* **1998**, *17*, 87−91.

(26) Licht, S. Semiconductor Electrodes and Photoelectrochemistry. In *Encyclopedia of Electrochemistry*; Bard, A. J., Stratmann, M., Eds.; Wiley-VCH: Weinheim, 2002; Vol. *6*, pp 3−47.

DOI: 10.1021/acsomega.9b02294
ACS Omega 2019, 4, 18279−18288

(27) Boldish, S. I.; White, W. B. Optical band gaps of selected ternary sulfide minerals. *Am. Mineral.* **1998**, *83*, 865−871.
(28) Wei, D. W.; Osseo-Asare, K. Semiconductor electrochemistry of particulate pyrite: mechanisms and products of dissolution. *J. Electrochem. Soc.* **1997**, *144*, 546−553.
(29) Mcmillan, R. S.; MacKinnon, D. J.; Dutrizac, J. E. Anodic dissolution of n-type and p-type chalcopyrite. *J. Appl. Electrochem.* **1982**, *12*, 743−757.
(30) Niu, X. P.; Ruan, R. M.; Tan, Q. Y.; Jia, Y.; Sun, H. Y. Study on the second stage of chalcocite leaching in column with redox potential control and its implications. *Hydrometallurgy* **2015**, *155*, 141−152.
(31) Zhang, L.; Su, F.; Wang, N.; Liu, S.; Yang, M.; Wang, Y. Z.; Huo, D. Q.; Zhao, T. T. Biodegradability enhancement of hydrolyzed polyacrylamide wastewater by a combined Fenton-SBR treatment process. *Bioresour. Technol.* **2019**, *278*, 99−107.
(32) Peiffer, J. A.; Spor, A.; Koren, O.; Zhao, J.; Tringe, S. G.; Dangl, J. L.; Buckler, E. S.; Ley, R. E. Diversity and heritability of the maize rhizosphere microbiome under field conditions. *Proc. Natl. Acad. Sci. U.S.A.* **2013**, *110*, 6548−6553.
(33) Edgar, R. C.; Haas, B. J.; Clemente, J. C.; Quince, C.; Knight, R. UCHIME improves sensitivity and speed of chimera detection. *Bioinformatics* **2011**, *27*, 2194−2200.
(34) Wang, Q.; Garrity, G. M.; Tiedje, J. M.; Cole, J. R. Naïve Bayesian classifier for rapid assignment of rRNA sequences into the new bacterial taxonomy. *Appl. Environ. Microbiol.* **2007**, *73*, 5261−5267.
(35) Wu, B.; Wen, J. K.; Chen, B. W.; Yao, G. C.; Wang, D. Z. Control of redox potential by oxygen limitation in selective bioleaching of chalcocite and pyrite. *Rare Met.* **2014**, *33*, 622−627.

DOI: 10.1021/acsomega.9b02294
ACS Omega 2019, 4, 18279−18288